Biol. Cybern. 84, 41–55 (2001)

Biological Cybernetics

Combined Hebbian development of geniculocortical and lateral connectivity in a model of primary visual cortex

A. P. Bartsch, J. L. van Hemmen

Physik Department T35, Technische Universität München, 85747 Garching bei München, Germany

Received: 20 December 1999 / Accepted in revised form: 9 June 2000

Abstract. We present a network model of visual map development in layer 4 of primary visual cortex. Our model comprises excitatory and inhibitory spiking neurons. The input to the network consists of correlated spike trains to mimick the activity of neurons in the lateral geniculate nucleus (LGN). An activity-driven Hebbian learning mechanism governs the development of both the network's lateral connectivity and feedforward projections from LGN to cortex. Plasticity of inhibitory synapses has been included into the model so as to control overall cortical activity. Even without feedforward input, Hebbian modification of the excitatory lateral connections can lead to the development of an *intracortical* orientation map. We have found that such an intracortical map can guide the development of feedforward connections from LGN to cortical simple cells so that the structure of the final feedforward orientation map is predetermined by the intracortical map. In a scenario in which left- and right-eye geniculocortical inputs develop sequentially one after the other, the resulting maps are therefore very similar, provided the intracortical connectivity remains unaltered. This may explain the outcome of so-called reverse lid-suture experiments, where animals are reared so that both eyes never receive input at the same time, but the orientation maps measured separately for the two eyes are nevertheless nearly identical.

1 Introduction

How does a cortical map arise? This is a longstanding question that has stimulated many experimental and theoretical investigations. On the one hand, it has been proposed that the layout of any map may be genetically coded. On the other hand, cortical maps may form through a Hebbian learning process driven by spontaneous or sensory-induced neuronal activity. Here we suppose that the basic network structure is made available by genetic coding and show how most of the orientation map in primary visual cortex can emerge from Hebbian plasticity of intracortical and geniculocortical interactions. Since the discussions concerning the origin of cortical maps are intense, we start with a short review.

Measurements of neuronal activity in primary visual cortex of cat have shown that cortical cells respond well to stimulation within a certain receptive field on the retina. Many cells respond preferentially to bar-like stimuli of a specific orientation and are activated predominantly through one of the two eyes. The location of the receptive field, the preferred orientation, and the ocular dominance of recorded cells change gradually as the recording site is moved tangentially to the cortical surface (Hubel and Wiesel 1962). The global organization of these cortical response properties has been mapped by anatomical, electrophysiological, and optical imaging methods for cat (Tusa et al. 1978; Bonhoeffer and Grinvald 1991; Bonhoeffer and Grinvald 1993), monkey (LeVay et al. 1975; Hubel et al. 1977; Blasdel and Salama 1986; Blasdel 1992a,b), ferret (Law et al. 1988; Chapman and Stryker 1993; Chapman et al. 1996; Weliky and Katz 1997), and tree shrew (Humphrey and Norton 1980; Humphrey et al. 1980; Bosking et al. 1997).

It is, however, still a matter of debate how cortical orientation selectivity is set up (Ferster and Miller 2000). Hubel and Wiesel (1962) originally proposed that geniculocortical connections are arranged so that the receptive field centers of thalamic cells projecting onto a single cortical simple cell cover an elongated region in the visual field. While there are many experimental studies claiming that the response properties of simple and complex cells are mainly determined by feedforward projections, as suggested by this model (Ferster 1987, 1988; Reid and Alonso 1995; Ferster et al. 1996; Chung and Ferster 1998), others find that intracortical links provide the main contribution (Sillito 1979; Sillito et al. 1980; Crook and Eysel 1992; Nelson et al. 1994). At

Correspondence to: A. P. Bartsch
(e-mail: Armin.Bartsch@physik.tu-muenchen.de)

present it seems most likely that both feedforward and recurrent intracortical processes both excitatory and inhibitory in nature participate in the formation of orientation selectivity (Vidyasagar et al. 1996).

Theoretical studies (von der Malsburg 1973; Linsker 1986a,b; Kammen and Yuille 1988; Stetter et al. 1993; Miller 1994; Wimbauer et al. 1997a,b) have proposed a Hebbian development of geniculocortical synapses that is driven by correlated feedforward input from thalamic neurons (for a recent review see Miller et al. 1999). In these correlation-based approaches, the intracortical connectivity is usually assumed to be rotationally symmetric and fixed. Under relatively general conditions they predict the emergence of an orientation map for cortical simple cells which is formed by the resulting arrangement of feedforward connections.

As such, the above explanation of cortical map formation has been challenged by work of Gödecke and Bonhoeffer (1996) and Sengpiel et al. (1998). In their experiments, cats were raised so that both eyes never received visual input at the same time, which was achieved by reverse lid suture. If geniculocortical refinement were driven by activity correlations in the lateral geniculate nucleus (LGN) and these correlations were mainly determined by the correlations of the visual input, then the left-eye orientation map would form independently of the right-eye map and the two maps could be expected to be different. Optical imaging of area 18, however, showed them to be nearly identical. The authors concluded that each map's layout was fixed by some internal mechanism either a priori or during the period when the first eye was open. They proposed long-range horizontal projections within primary visual cortex as a potential substrate of this mechanism.

Recently, however, Erwin and Miller (1998) have demonstrated that the emergence of ocularly-matched orientation maps can be well explained within the framework of correlation-based development, if an appropriate amount of thalamic inter-eye activity correlations is assumed. Experimental findings of Weliky and Katz (1999) indicate that strong inter-eye correlations are indeed present in the ferret's LGN before eye opening. Nevertheless, it is still unclear whether this model can actually account for the outcome of the reverse lid-suture experiments.

Wolf et al. (1996) have pointed out that cortical area 18 of the cat is shaped as a narrow band on the cortical surface, so that pattern formation within this region is subject to strong confinement. In computer simulations they have shown that different feedforward orientation maps developing under this constraint are always very similar – in accordance with reverse-suturing experiments. The authors argued that experimental results should be qualitatively different in a larger area, e.g. area 17, because boundary conditions are less important. As Bonhoeffer and Gödecke (1996) have explained: ''Unfortunately this idea is difficult to test, as in cats the main part of area 17 lies buried in the medial bank and is therefore inaccessible to optical imaging''.

In this paper we propose a model of layer 4 of primary visual cortex consisting of laterally interconnected *spiking* neurons of both excitatory and inhibitory type. It combines the idea of correlation-based learning of geniculocortical afferents with Hebbian development of short-range intracortical synapses. Inhibitory interneurons and plastic inhibitory synapses have been included in the model so as to control overall network activity.

Large-scale computer simulations show that in this kind of network it is possible to obtain an *intracortical* orientation map from a Hebbian learning process driven by cortical activity alone. The process does not depend on the presence of feedforward input and could therefore occur at early stages of visual development, when thalamic axons have not yet entered cortical layer 4. The resulting map structure resembles that typical of orientation maps obtained from optical imaging experiments. This might indicate that intracortical circuitry does contribute significantly to the orientation selective response properties of cells in the primary visual cortex.

Experiments by Ferster (Ferster 1987, 1988; Ferster et al. 1996) do indicate, however, that feedforward input from the LGN is relevant as well. Consistently with these data, we demonstrate that correlation-based development of geniculocortical projections can interact with emerging intracortical connectivity so as to give a matched feedforward and intracortical orientation tuning for each cortical cell. As a consequence, the developing pattern of feedforward projections is more or less predetermined once the intracortical connectivity is fixed. This provides a very natural explanation for the remarkable stability of orientation maps that has been found experimentally (Kim and Bonhoeffer 1994; Weliky and Katz 1997; Gödecke and Bonhoeffer 1996; Sengpiel et al. 1998, 1999). In contrast to the proposition of Wolf et al. (1996), our model predicts strong correlation between orientation maps in reverse-suturing experiments not only for small but also for larger visual areas such as area 17 of the cat.

This paper is organized as follows. In Sect. 2 we introduce the model of spiking neurons that we have used in our simulations. We then turn to a description of the full network, explain the learning rules that govern synaptic development, and finally we present our data-analyzing procedure. In Sect. 3 we show that intracortical orientation maps can develop from spontaneous cortical activity alone, without feedforward input. We demonstrate how this intracortical development can be combined with plasticity of geniculocortical connectivity and show that such a combined development can explain the outcome of the reverse-suturing experiments. We end with a summary and a short discussion.

Part of this work has been presented in preliminary form – see Bartsch and van Hemmen (1999).

2 Methods

2.1 Spiking neurons

To keep our network as close to biology as possible, we decided to build it up from spiking neurons. A neuron model that is able to reproduce many biological features

and yet allows large network simulations is given by the usual integrate-and-fire neuron. For the present investigation we have chosen the stochastic spike response model (Gerstner and van Hemmen 1992, 1994), which is a more flexible, extended version of the integrate-and-fire neuron.

The state of a spike-response neuron is described by its membrane potential h as a function of time. Every incoming spike evokes a transient change of this membrane potential called postsynaptic potential and modeled as a response kernel $\varepsilon(t)$. After spike emission the neuron enters a refractory period that is described by a second response function $\eta(t)$, the refractory potential. Spike generation itself is governed by a generalized Poisson process. This means that the probability $P^{\mathrm{f}}(t, \mathrm{d}t)$ that the neuron emits a spike during the infinitesimal time interval $[t, t+\mathrm{d}t]$ can be written

$$P^{\mathrm{f}}(t, \mathrm{d}t) = \lambda(t)\mathrm{d}t \ ,$$

and the probability of more than one spike being emitted during that period is $o(\mathrm{d}t)$. The spike emission rate $\lambda(t)$ is given by some function q of the membrane potential h,

$$\lambda(t) = q[h(t)] \ .$$

Each time the neuron generates an action potential, a negative contribution $\eta(t)$ is added to the membrane potential to account for the reduced excitability during the refractory period. At a postsynaptic neuron i each action potential arriving from a presynaptic neuron j induces a postsynaptic potential that is given by $\varepsilon(t)$ multiplied by a synaptic weight J_{ij}.

Thus the total membrane potential h_i of neuron i is a sum of a synaptic contribution h_i^{syn} evoked by spikes of other neurons and a refractory contribution h_i^{refr} as a result of its own spiking:

$$h_i(t) = h_i^{\mathrm{syn}}(t) + h_i^{\mathrm{refr}}(t) \ ,$$

where

$$h_i^{\mathrm{refr}}(t) = -\sum_{t_i^{\mathrm{f}} \le t} \eta\left(t - t_i^{\mathrm{f}}\right) \ ,$$

$$h_i^{\mathrm{syn}}(t) = \sum_j \sum_{t_j^{\mathrm{f}} \le t} J_{ij}\varepsilon\left(t - t_j^{\mathrm{f}}\right) \ ,$$

and t_i^{f} denotes the firing times of neuron i.

2.2 Network setup and simulation algorithm

We have designed a network of spike response neurons that is intended to model: (a) excitatory and inhibitory cells in a small patch of layer 4 in primary visual cortex, and (b) excitatory cells in a corresponding patch of LGN, providing input to cortical layer 4. The full network is separated into three equally-sized square grids with periodic boundary conditions (see Fig. 1).

Cortical excitatory and inhibitory cells make up two of these grids. We have separated them into distinct layers so as to clarify the connectivity structure within the network; we do not presume that such a separation is present anatomically. We assume that every neuron has a limited arborization range of axon collaterals and dendrites within layer 4 so that each excitatory neuron receives lateral connections from a certain region of neighbouring excitatory cells as well as from a region of neighbouring inhibitory cells. With the network being intended for an investigation of developmental processes occurring relatively early in cortical layer 4, the long-range excitatory connections found in laminae 2/3 and 5 are neglected. It is therefore plausible to choose similar arborization regions for both excitatory and inhibitory connections. Here these regions have been chosen to be circles centered on the cell under consideration and extending over 11 cells in diameter – a number that is not realistic but suffices for simulation purposes. In the present version of our model, inhibitory neurons receive lateral excitatory input from within a neighbourhood of 11 neurons in diameter, but do not make synapses with

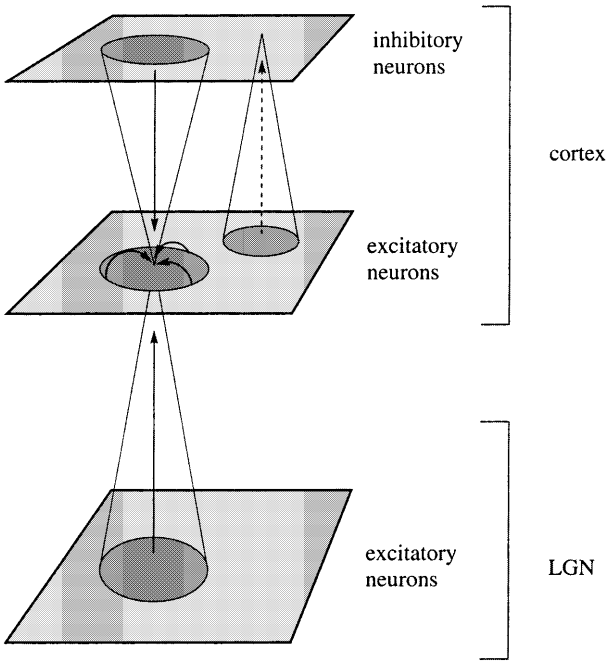

Fig. 1. The network model we use to study intracortical and feedforward learning dynamics can be decomposed into three equally-sized square grids of spike response neurons. The two upper layers are designed to represent a small patch of layer 4 of primary visual cortex. Excitatory and inhibitory neurons have been separated into distinct layers only for a clear illustration of the connectivity structure. We do not presume that such a separation is present anatomically. Each of the excitatory cortical neurons receives lateral input from neighbouring excitatory and inhibitory cortical cells. Inhibitory neurons are driven by the activity of excitatory neurons. Feedforward input into the cortex is provided by LGN neurons in the bottom layer, representing geniculate relay cells. They produce correlated spike activity with known statistics. All synaptic connections except for those from excitatory to inhibitory cells (dashed arrow) are subject to activity-driven learning dynamics. Periodic boundary conditions have been applied throughout each layer. In that part of our simulations where we consider cortical learning dynamics alone (Sect. 3.1), the LGN grid is not present so that we are left with the two upper layers only

other inhibitory cells. They produce an inhibitory background of spikes that is used to normalize overall network activity.

A third layer in our setup represents geniculate cells, providing input to the cortex. Since in this paper investigations are restricted to the case of monocular input, we need only consider neurons located within one eye-specific lamina in the LGN, say lamina A. Every excitatory cortical neuron obtains input from geniculate neurons lying within a circular arborization area centered at the retinotopic position of the cortical cell. Again the diameter of the circle extends over 11 neurons. To save computation time, which is an important limiting factor of our simulations, we only model LGN cells with ON-center receptive fields and do not account for OFF-center cells explicitly. It will become clear in the following text why this is possible. All synaptic connections in the network, except for those from excitatory to inhibitory cells (dashed arrow), are subject to activity-driven learning dynamics.

In many existing models of correlation-based geniculocortical self-organization (Linsker 1986b; Miller 1994; Wimbauer et al. 1997a,b; Erwin and Miller 1998), orientation selectivity of simple cells develops through a competition between inputs from LGN neurons with ON-center and OFF-center receptive fields. Correlated random activity of geniculate cells is the driving force for this competition. The typical simple-cell receptive field structure emerging from such a model can be understood to be the result of a symmetry-breaking process taking place separately for ON- and OFF-center inputs. This three-stage process is illustrated in Fig. 2 from left to right.

In our model, like in previous ones, the emergence of orientation selectivity in the geniculocortical projections is driven by correlated random activity of LGN cells. Since, however, ON-OFF competition can be viewed as two coupled but separable symmetry-breaking processes, we take into account only one geniculate cell type, with ON-center receptive fields, say. It should be emphasized, though, that we do *not* presume that OFF-center LGN cells do not contribute to orientation selectivity. Neglecting OFF-center inputs in our model is simply a computational shortcut. Because of the aforementioned anticorrelations between ON-center and OFF-center activities, in Fig. 2 the complete receptive field structure shown by (c) is fully determined by either one of the two substructures displayed by (b). It is therefore sufficient to study the development of geniculocortical synapses from either ON- or OFF-center LGN cells. The lower part of Fig. 2b gives a schematic view of a simple cell's typical feedforward input connectivity emerging in our reduced model.

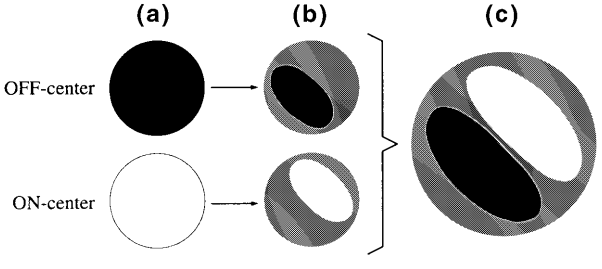

Fig. 2. Emergence of an orientation selective simple-cell receptive field through competition between inputs from LGN neurons with ON- and OFF-center receptive fields. Initially the cell receives input of both ON- and OFF-center type from a circularly symmetric region in the visual field, indicated by a white and a black circle, respectively (a). In the course of a symmetry breaking process, both input types become restricted to non-isotropic *subfields* (b). This symmetry breaking can be thought of as occurring separately for ON- and OFF-center inputs. An assumed anticorrelation between the activities of the two geniculate cell types ensures that the *subfields* are in anti-phase with each other. Together they form the receptive field shown on the right (c), where a black or a white shading indicates whether dominant input is from OFF- or ON-type cells

In short, the simulation algorithm that has been applied is as follows. At the beginning of each time step, the firing probability of every neuron is determined from its membrane potential h. To be specific, we let

$$P\{\text{spike during } \Delta t \,|\, h\} \approx q(h)\Delta t = \{1+\exp[-(h-\theta)/T]\}^{-1} = (1/2)\{1+\tanh[(h-\theta)/2T]\} \ , \quad (1)$$

with $\Delta t = 1$ ms denoting the size of the time step, θ being the neural threshold and T a noise parameter.

Next, it is decided randomly from the firing probability whether a neuron emits a spike or remains silent during the current time step. Subsequently, the membrane potential of each cell is updated using the spike trains of all the neurons projecting onto it. Both the postsynaptic potential $\varepsilon(t)$ and the refractory potential $\eta(t)$ have been chosen to be exponentials (see Fig. 3):

$$\varepsilon(t) = \exp(-t/\tau_\varepsilon) \ , \quad (2)$$

$$\eta(t) = \eta_0 \exp(-t/\tau_\eta) \ , \quad (3)$$

for $t > 0$ and vanishing for $t \le 0$, with $\tau_\varepsilon = 6$ ms, $\tau_\eta = 10$ ms, and $\eta_0 = 10$. At the end of each time step, all synaptic weights are modified as is explained in Sect. 2.3.

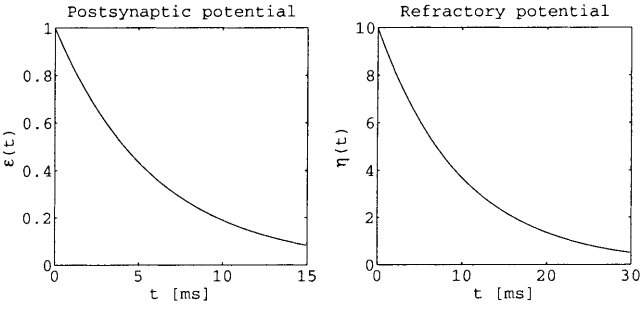

Fig. 3. In the spike response model (cf. Sect. 2.1) every incoming spike induces a transient change of the postsynaptic neuron's membrane potential. This postsynaptic potential is described by a response function $\varepsilon(t)$, which we have chosen to be an exponential as displayed in the left panel. To model refractoriness, a second response kernel $\eta(t)$, shown in the right panel, is subtracted from the membrane potential after spike emission

In order to simulate correlated thalamic activity the membrane potentials of the LGN neurons are prescribed externally. Their values are drawn from a two-dimensional Gaussian random field. A new realization of this random field is generated every 10 time steps. In this simple way we obtain spatially and temporally correlated spike trains from LGN neurons.

Depending on the simulation, these steps are repeated for 2 500 000 or 5 000 000 iterations (see simulation parameter values in the Appendix), which corresponds to roughly 40 or 80 minutes in real time.

2.3 Learning mechanisms

There is increasing evidence that synaptic plasticity in the developing brain is to a large extent dependent on neural activity (Wiesel and Hubel 1963; Crair et al. 1998; Issa et al. 1999). Originally, Hebb (1949) postulated that the efficacy of a connection between two cells is increased if the postsynaptic cell is repeatedly activated by the presynaptic one. Since then many studies have shown that by appropriately coactivating a pair of neurons, the strength of their connection can indeed be modified (Brown and Chattarji 1994; Fregnac et al. 1994).

In the model presented in this paper we have incorporated plasticity of both excitatory and inhibitory connections. Modification of *excitatory* synapses is governed by the following rules:

1. A Hebbian mechanism increases synaptic efficacy whenever a presynaptic action potential is immediately followed by a postsynaptic one (see the learning window in Fig. 4).

2. Each time a neuron emits a spike, the weights of all its incoming synapses are reduced by a certain amount. Such a process prevents a neuron from enhancing its inputs ad infinitum, since growing input increases the neuron's firing rate, which in turn diminishes the weight of incoming synapses. As a consequence, different input synapses of the same neuron have to compete for synaptic weight, because an increased efficacy of one group of synapses leads to a down-regulation of the remaining ones due to the cell's increased firing rate. Experimental support for this mechanism has been provided by work of Turrigiano et al. (1998), who found the total input strength of rat cortical pyramidal cells to be increased or decreased as a function of activity.

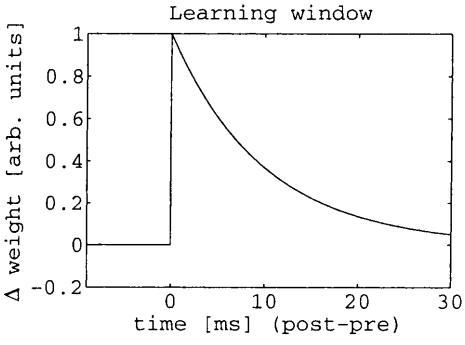

Fig. 4. Learning window $W(t)$ for excitatory synapses. In our model, an excitatory synapse is strengthened whenever a presynaptic spike is immediately followed by a postsynaptic one. The graph displays the change of synaptic weight (in arbitrary units) that is applied depending on the time difference between the post- and presynaptic spikes

Taken together, the rules 1. and 2. cause a synapse to be up-regulated when a postsynaptic spike immediately follows a presynaptic one, and to be down-regulated otherwise. This is at least in qualitative agreement with experimental findings (Markram et al. 1997; Zhang et al. 1998).

3. The efficacy of every synapse is slowly reduced at a rate proportional to its current weight. Recently, Engert and Bonhoeffer (1999) gave some indirect evidence for such an activity-independent decay in rat hippocampal slice cultures.

4. Each synaptic weight is enhanced at a constant rate, independent of neuronal activity. Together with rule 3., this means that without activation a synapse will slowly approach some non-zero efficacy. This process can be considered as an activity-independent formation of synapses that is driven by some sort of nerve growth factor.

5. Finally, we limit each synaptic weight to a finite range between 0 and some upper bound. Note, however, that in contrast to some previous models (Miller 1994; Wimbauer et al. 1997a,b; Erwin and Miller 1998) these bounds are not sticky, i.e. all synapses remain plastic, whether they are saturated or not.

With $J^{\mathrm{e}}_{ij}(t)$ denoting the excitatory weight from neuron j to neuron i, the change $\Delta J^{\mathrm{e}}_{ij}(t)$ that results from contributions by rules 1. to 4. to this weight during the current time step can be summarized in the following formula:

$$\Delta J^{\mathrm{e}}_{ij}(t) = A^{\mathrm{e}}_{ij}\Bigg[\underbrace{a_i(t)\sum_{t^{\mathrm{f}}_j<t} W\left(t-t^{\mathrm{f}}_j\right)}_{(1)} + \underbrace{a_i(t)\sigma^{\mathrm{e}}}_{(2)} + \underbrace{\xi^{\mathrm{e}}}_{(4)}\Bigg] - \underbrace{\vartheta^{\mathrm{e}} J^{\mathrm{e}}_{ij}(t)}_{(3)} \quad . \tag{4}$$

In this expression, $W(t)$ denotes the learning window (see Fig. 4)

$$W(t) = \exp(-t/\tau_W) \quad , \tag{5}$$

where $\tau_W = 11$ ms, and $a_i(t)$ is the activity of neuron i at the current time step, with $a_i(t) = 1$ if an action potential is emitted and $a_i(t) = 0$ otherwise. As in Sect. 2.1, the t^{f}_i indicate the firing times of cell i. Below each term, the corresponding number of the above list of items is given.

In real cortex, the number of synapses connecting two neurons as a function of their distance is probably a random quantity (Braitenberg and Schüz 1991). A similar argument may hold for the connections from thalamic relay cells to cortical neurons and their respective retinotopic coordinates. However, in our simulations we

neglect the statistical nature of this process. Instead, we have introduced an 'arbor function' A^{e}_{ij}, expressing the expected number of synapses between the neurons j and i. Within this framework, J^{e}_{ij} is taken to be the effective weight connecting cell j to cell i, i.e. the efficacy of a single synapse multiplied by the number of synapses from j to i.

In addition to the above learning rules, an unspecific spread of weight changes onto neighbouring but non-activated synapses can be included in the model, as is suggested by measurements of Engert and Bonhoeffer (1997). Although the results presented in this paper have been obtained without this kind of plasticity, we have performed a corresponding set of numerical simulations where such an unspecific modification of excitatory synapses has been taken into account. Except for a smoothing of the emerging connectivity patterns, we did not find a qualitative change in our results.

To control overall activation, i.e. to avoid epileptiform bursts, our network takes advantage of the subsequent learning rules for *inhibitory* connections:

1. Whenever an excitatory neuron of the cortical layer generates an action potential, its incoming inhibitory synapses are enhanced by a certain amount. This implements a negative feedback loop with a higher firing rate leading to a cell receiving more inhibition, thereby limiting its activity.
2. The efficacy of every synapse is slowly reduced at a rate proportional to its current weight.
3. The upper bound of zero prevents inhibitory weights from becoming excitatory. In contrast to excitation, there is no lower bound for inhibition.

Using the same notation as above and neglecting the zero upper bound, the change of the inhibitory efficacy $J^{i}_{ij}(t)$ that results during one time step can be written

$$\Delta J^{i}_{ij}(t) = -A^{i}_{ij}\underbrace{a_i(t)\sigma^{i}}_{(1)} - \underbrace{\vartheta^{i}J^{i}_{ij}(t)}_{(2)} \quad . \tag{6}$$

Again, we have used an arbor function A^{i}_{ij} to express the expected number of synapses that the inhibitory neuron j makes onto cell i. It should be noted that, within the framework of the spike response model, inhibitory synapses are represented by a negative coupling constant J_{ij}. To strengthen an inhibitory synapse is thus equivalent to making its weight J_{ij} more negative, which is the reason for the negative sign in front of the first term.

In order to allow inhibition to respond sufficiently fast to changes of excitation during synaptic development, parameters have been chosen so that the typical relaxation time of inhibitory weights is significantly shorter than that of excitatory weights. More specifically, we let $\vartheta^{e} = 2.5 \times 10^{-6}$ for excitatory intracortical synapses, $\vartheta^{e} = 1.25 \times 10^{-6}$ for geniculocortical synapses, and $\vartheta^{i} = 10^{-4}$ for inhibitory synapses, corresponding to relaxation time constants of 400 s, 800 s, and 10 s, respectively.

Comparing these time constants with the typical time course of pattern formation in the visual system of higher mammals during the critical period, it is obvious that Nature takes more time for development than we do in our simulations. Unfortunately, numerical simulations with spiking neurons are computationally very expensive, meaning that at the moment it is impossible to run simulations of suitably sized networks representing periods of a week or more in real time. We thus have to reduce the relevant time constants and speed up learning. In our experience, however, the process of pattern formation does not become instable, but rather more stable as learning is slowed down. This is reasonable since reducing the speed of learning means averaging over a larger number of pre- and postsynaptic spikes, which reduces the effects of noise. We therefore think that the results presented below could be reproduced using realistic biological learning time constants by simply rescaling time.

2.4 Data analysis

In Sect. 3 we investigate the connectivity structures emerging from the learning mechanisms in the network described so far. To this end, we focus on the incoming excitatory synapses of all excitatory neurons. As it turns out, these coupling structures very often show an elongated shape of a certain orientation. Here the method is described that we have applied to determine these orientations.

In our model, the excitatory input efficacies of one cortical cell, say at location $(0,0)$, are given as a two-dimensional synaptic array $\tilde{J}_{xy}$ of 11×11 positive real values. Here the coordinates (x,y) can range through either the geniculate or the cortical layer while the reference point $(0,0)$ is in V1 (cf. Fig. 1). In order to obtain the orientation of a connectivity pattern, we calculate the overlap of the corresponding synaptic array with a set of Gaussian 'bars' S_{xy}:

$$S_{xy}(\phi,p) := \exp\left\{\frac{-[x\cos\phi + y\sin\phi - p]^2}{2\cdot 0.5^2}\right\} \times \exp\left\{\frac{-[-x\sin\phi + y\cos\phi]^2}{2\cdot 4^2}\right\} - S_0(\phi,p) \quad ,$$

where $x,y \in \{-5,-4,\ldots,5\}$. The parameter ϕ determines the orientation of the bar and p controls its position within a frame of 11×11 pixels. $S_0(\phi,p)$ is chosen so that $\sum_{xy} S_{xy}(\phi,p) = 0$. For each of the four orientations $\phi \in \{0^\circ, 45^\circ, 90^\circ, 135^\circ\}$, p is varied to determine the maximal overlap:

$$R(\phi) := \max_{p}\left[\sum_{x,y}\tilde{J}_{xy}S_{xy}(\phi,p)\right] \quad .$$

These values are then taken as the lengths of four vectors $\vec{x}(\phi)$ pointing in the directions given by 2ϕ, i.e.

$$\vec{x}(\phi) := [R(\phi), 2\phi]$$

in polar coordinates. We sum the four vectors so as to obtain a polar vector

$$\vec{y} = (R_y, \psi_y) := \vec{x}(0^\circ) + \vec{x}(45^\circ) + \vec{x}(90^\circ) + \vec{x}(135^\circ) \ ,$$

and take the resulting polar angle ψ_y divided by two as the required orientation ϕ^{or} of the synaptic weight pattern,

$$\phi^{\mathrm{or}} := \psi_y/2 \ .$$

The described procedure is a formal method to analyze the neuronal connectivity. It does not directly yield the cells' preferred orientation as it would be measured in an optical imaging experiment. To achieve this, we would have to apply test stimuli to the geniculate layer of our network and record the activity in the cortical layer. The obtained neural response properties would then be determined by the feedforward connectivity, the lateral connectivity, and the nonlinear gain function. In this work, however, we focus on the developmental interplay of feedforward and lateral projections and thus have to investigate their structures separately.

3 Results

We now present the results obtained from different simulations of our model network. Since the number of simulation parameters is relatively large, we will give only a qualitative description in the main text. For the complete network setup the reader is referred to the Appendix, where the relevant parameter values are listed.

3.1 Intracortical self-organization

Anatomical studies of the cat's developing visual system (Shatz and Luskin 1986; Gosh and Shatz 1992) have revealed that geniculate axons have reached the cortical subplate by embryonic day (E) 36 but do *not* enter the future cortex during the following week. Although most of the cells destined for cortical layer 4 have finished their migration by E55, a geniculate projection to layer 4 could only be detected by E60. Thus, for layer 4 of area 17 in the cat, there is likely to be a waiting period of about 1 week between the completion of neuronal migration and thalamic innervation. This suggests the possibility of an intracortical synaptic refinement occurring for about one week *without* feedforward input from LGN.

As long as the primary visual cortex does not receive external input, spike-spike correlations of spontaneous activity are determined by lateral interactions. If the lateral connections are shaped by an activity-driven Hebbian learning rule, as we assume in our model, their development is in turn determined by the cortical spike-spike correlations. It is therefore interesting to know what the connectivity patterns emerging under these conditions will look like.

In order to investigate this, we used the network described in Sect. 2.2 but removed the geniculate layer. It turned out that under certain conditions of network activity the development of excitatory lateral projections can undergo a symmetry breaking process. As a result, every neuron will receive most of its lateral input from neighbouring excitatory cells lying within an elongated region of a certain orientation. Without this symmetry breaking process the emerging patterns of connectivity will be rotationally invariant. Both cases are illustrated schematically for one excitatory cell in Fig. 5.

Figure 6 presents the outcome of two different runs of a network comprising 16×16 excitatory and an equal number of inhibitory neurons. Lateral input is restricted to a circular region of 11 cells in diameter, as explained in Sect. 2.2, i.e. synaptic weights from neurons outside this circle are zero and the corresponding pixels are black. For the first network run (Fig. 6a), we have chosen a low value for the parameter ξ^{e} in Eq. 4. The emerging coupling patterns are rotationally symmetric. For the second run (Fig. 6b), ξ^{e} has been increased, resulting in higher synaptic efficacies on average. In this case, rotational symmetry is broken during the learning process and the emerging connectivity patterns obtain an elongated shape.

To each of these elongated patterns an orientation can be assigned as described in Sect. 2.4. Figure 6c visualizes the resulting array of orientations. For every neuron, a small rectangle is plotted with a color coding for the orientation of the corresponding input connectivity pattern. The continuous color code that has been applied is indicated for a few orientations below the plot.

In Fig. 7 we display the lateral projections that have emerged in a simulated network whose grid size was 32×32. The global structure of the map resembles that of typical orientation maps obtained from optical imaging experiments in primary visual cortex (Bonhoeffer and Grinvald 1991; Blasdel 1992b; Bonhoeffer and Grinvald 1993; Chapman et al. 1996; Bosking et al.

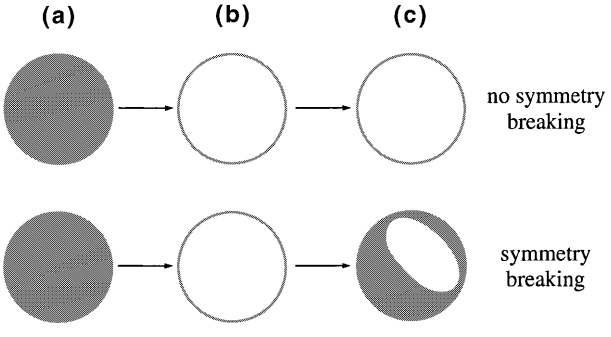

Fig. 5. The panels (a) to (c) display different developmental stages of a cortical cell's intracortical input that can arise in our model. The cell receives lateral excitatory projections from neurons within a circular arborization area. In the different panels of this figure, the outline of the arborization area is shaded according to the synaptic efficacy of the corresponding inputs. Projections from dark regions are weak whereas those from white regions are relatively strong. At the beginning of our simulations, all synaptic weights are zero (a). As the development proceeds, the neuron continually receives more and more input from within its circular arborization radius (b). Under certain conditions depending on network activity an oriented connectivity pattern will emerge due to a symmetry breaking process (bottom of panel c). Otherwise the input region will remain rotationally symmetric (top of panel c)

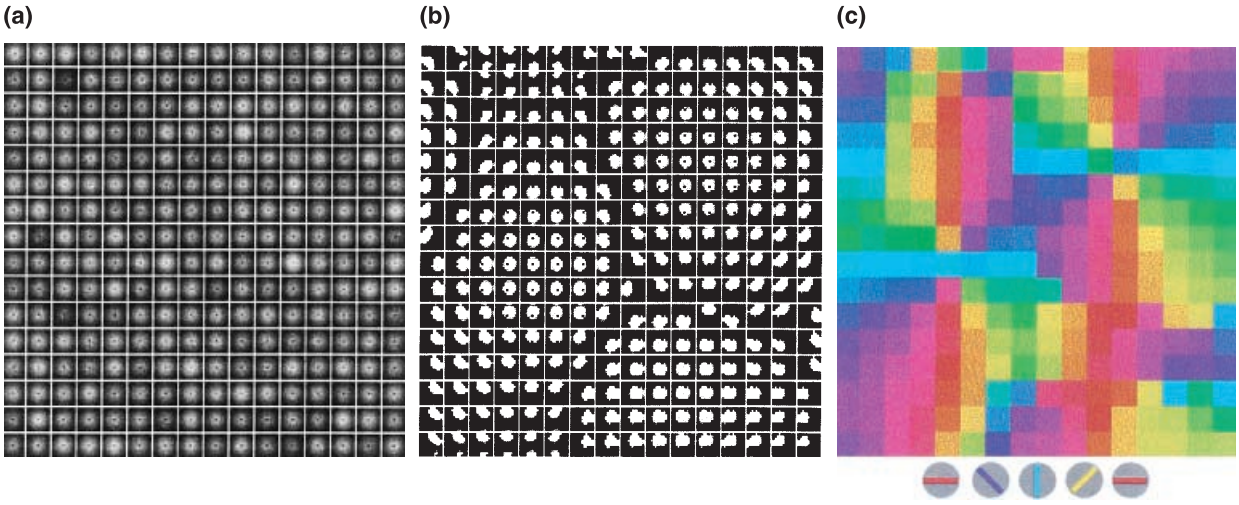

Fig. 6. The outcome of two different simulations of a network without feedforward input. It comprises 16×16 excitatory and an equal number of inhibitory neurons. **a**, **b** Visualization of the final excitatory lateral connectivities by means of two arrays of 16×16 grey level plots. In these plots, each of the small squares consists of 11×11 pixels, representing one cell's incoming synaptic weights from 11×11 neighbouring neurons. Dark and bright shaded pixels indicate low and high synaptic efficacies, respectively. For **a** we have chosen a low value of the parameter ξ^e in Eq. 4. The emerging coupling patterns are rotationally symmetric. For **b** ξ^e has been increased, resulting in higher synaptic efficacies on average. In this case, rotational symmetry is broken during the learning process and the emerging connectivity patterns obtain an elongated shape. As described in Sect. 2.4, an orientation can be assigned to each of these elongated patterns. **c** Visualization of the resulting array of orientations. For every neuron, a small rectangle is plotted with a color coding for the orientation of the corresponding input connectivity pattern. The continuous color code that has been applied is indicated for a few orientations below the plot

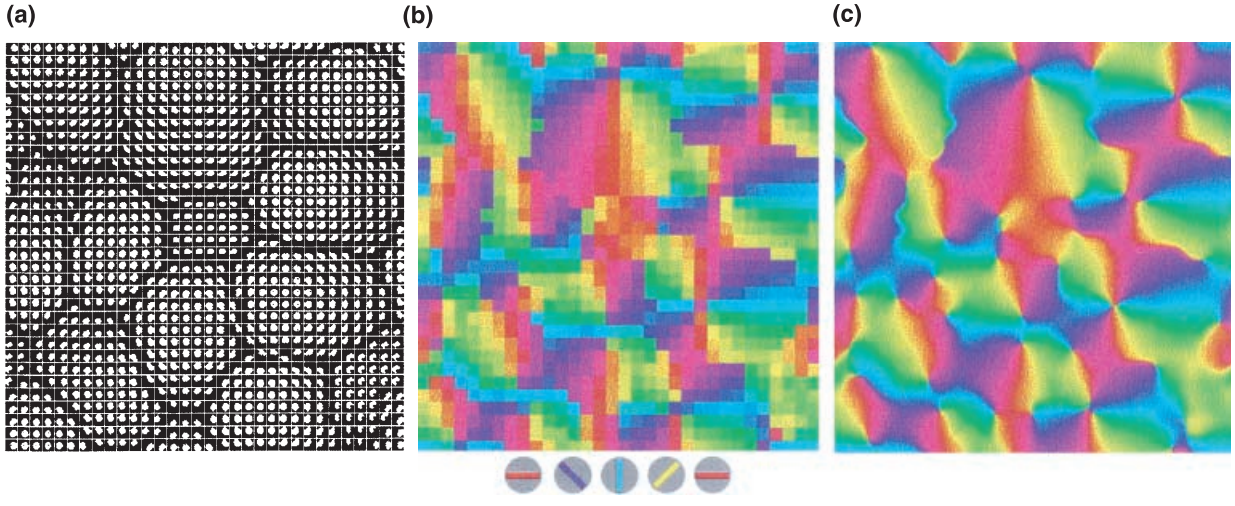

Fig. 7. The intracortical projections that have emerged from Hebbian learning in a network without geniculocortical input and with a grid size of 32×32 cells are presented as **a** grey level plots and **b** as a colored orientation map. **c** smoothed version of (b). The color code is the same as in Fig. 6

1997). This is even more obvious in Fig. 7c, where a smoothed version of Fig. 7b is presented. It can be seen clearly that orientation normally changes continuously across the surface of the simulated cortical patch. The only exceptions are point-like singularities where orientation changes by 90 degrees. Such singularities are well-known from experimental maps of preferred orientation and have been termed 'orientation centers' or 'pinwheel centers' (Bonhoeffer and Grinvald 1993). Around each of these pinwheel centers, every orientation is represented once. Two kinds of pinwheels can be distinguished according to whether orientation changes clockwise or counterclockwise around the center. Both kinds appear in approximately equal numbers per unit area of simulated cortical surface. This is again in agreement with experimental findings.

Our simulations demonstrate that a Hebbian learning mechanism driven by spontaneous activity can generate oriented patterns of intracortical connectivity. The overall organization of this connectivity can be considered as an intracortical orientation map that is similar to maps of preferred orientation that have been measured

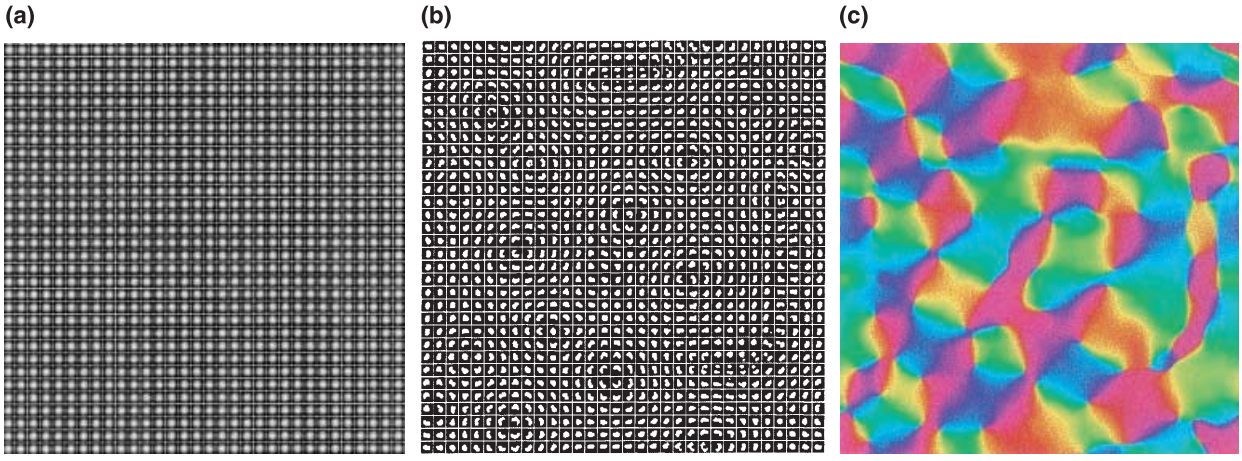

Fig. 8. An activity-driven development of geniculocortical afferents in the presence of an isotropic intracortical connectivity leads to the emergence of a feedforward orientation map; grid size is 32×32. This confirms the results of earlier studies carried out in models that used graded-response neurons and/or did not distinguish between excitatory and inhibitory cells. For each excitatory cortical cell, **a** displays the lateral input strengths as a grey level plot, and similarly **b** visualizes the efficacies of the feedforward input synapses from the LGN. Extracting orientations as described in Sect. 2.4, this feedforward connectivity pattern can be transformed into a color coded orientation map, which is shown in a smoothed version in **c**. The color code is the same as in Fig. 6

in striate cortex. This suggests that lateral projections may play an important role in the shaping of orientation-selective response properties of cells in the primary visual cortex. On the other hand, experimental data obtained by Ferster (Ferster 1987, 1988; Ferster et al. 1996) indicate that the feedforward connectivity from the LGN to the cortex also provide a significant contribution to simple-cell responses. In the present work, we therefore assume that a cortical neuron's orientation preference is set up by a combination of both its intracortical and its feedforward connections.

3.2 Combined feedforward and intracortical plasticity

We now investigate the effect that the existence of an intracortical orientation map can have on the development of geniculocortical feedforward projections. To this end, we activate the geniculate layer (that had been removed for the analysis in Sect. 3.1) and let the geniculocortical connections evolve according to the Hebbian learning dynamics described in Sect. 2.3. During that process, the pattern of excitatory intracortical projections is kept fixed, whereas inhibitory synapses remain plastic. This inhibitory plasticity allows for a normalization of overall network activity on short time scales and thus helps to avoid epileptiform discharges by shifting the balance of cortical excitation and inhibition towards an increased inhibition (Douglas et al. 1995; Varela et al. 1999).

As a first step we assume the lateral excitatory connections to have rotational symmetry, which corresponds to the scenario studied in earlier work (Linsker 1986a; Miller 1994; Wimbauer et al. 1997a,b; Choe and Miikkulainen 1998; Erwin and Miller 1998). These analyses were based on graded-response neurons and/or did not distinguish between excitatory and inhibitory cortical cells, whereas the present network consists of spiking neurons with inhibition mediated via inhibitory interneurons. It is therefore important to check whether previous results can be reproduced in our setup, which is closer to biology.

Figure 8a visualizes each excitatory cell's intracortical synaptic efficacies in the form of grey-level plots (see Fig. 6 for details). Grid size is 32×32 cells. As mentioned above, the coupling patterns have been chosen to be rotationally invariant, namely shaped as a two-dimensional Gaussian. The result of a simulation of geniculocortical development in this setup is presented in Fig. 8b. It shows an array of 32×32 grey level plots, each corresponding to the feedforward input connectivity of one excitatory cortical neuron. All these small plots consist of 11×11 pixels representing the efficacies of the input synapses that an excitatory cortical neuron receives from the LGN. A dark-shaded pixel means that the corresponding synapse is weak, whereas a white-shaded pixel indicates a strong synapse. All pixels outside a circle of diameter 11 are black, because the arborization area of the geniculocortical projection is a circle of that diameter, i.e. the synaptic efficacy from any LGN cell outside this area is zero.

Obviously, most of the excitatory cortical neurons receive their feedforward input from elongated patches on the LGN grid. As we have described in Sect. 2.2, these patches can be considered as the ON-center part of an orientation selective simple-cell receptive field. To extract the orientation of the connectivity pattern we apply the same method that we have used for the intracortical projections and which has been explained in Sect. 2.4.

We find that the feedforward orientation map shown in Fig. 8c is in good qualitative agreement with experimental data (Bonhoeffer and Grinvald 1991, 1993). This demonstrates that the results of previous models of correlation-based geniculocortical development can be nicely reproduced in our more detailed approach

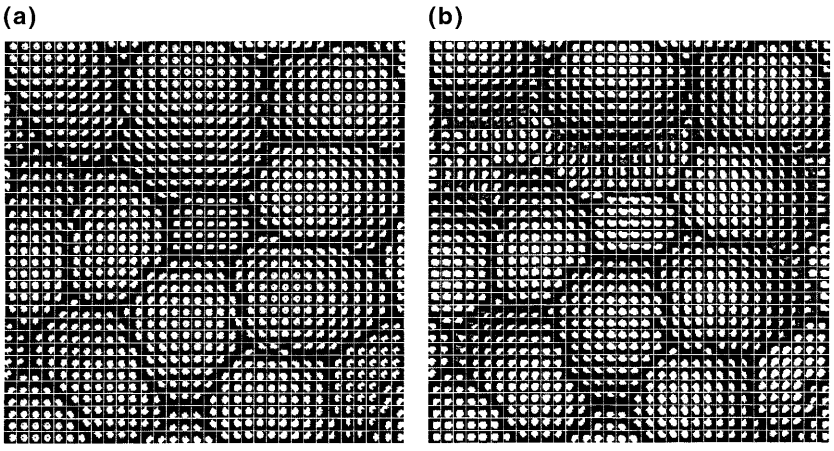

Fig. 9. **a** Same intracortical map as Fig. 7a. When feedforward connectivity develops in the presence of such an intracortical map, the resulting feedforward orientation map (shown in **b**) is essentially in agreement with the intracortical pattern, as can be seen from the similarity between the two images

(Bartsch and van Hemmen 1999, preprint; A. Bartsch and H. van Hemmen, in preparation).

Now we turn to the case of an anisotropic intracortical connectivity. We assume this connectivity to form an orientation map which has emerged during a preceding learning process as described in Sect. 3.1. To be specific, we use the map of Fig. 7. The efficacies of the intracortical excitatory synapses are fixed at their respective values while the spontaneous activity of the thalamic relay cells drives the development of geniculocortical feedforward projections. The grey-level coded results are presented in Fig. 9.

Figure 9a reproduces the intracortical map and Fig. 9b displays the final feedforward orientation map. The maps are very similar. This means that, in our model, a pre-existing intracortical connectivity can guide the synaptic refinement of geniculocortical afferents (Bartsch and van Hemmen 1998a; A. Bartsch and H. van Hemmen, in preparation). As a consequence, each cortical cell's final orientation preference – shaped by both its lateral and its feedforward connections – is highly determined by the intracortical orientation map that is present during the period of geniculocortical plasticity. This may provide a natural explanation for the enormous stability of orientation maps that has been found in experiments in which normal geniculocortical development is disturbed (Kim and Bonhoeffer 1994; Gödecke and Bonhoeffer 1996; Weliky and Katz 1997; Sengpiel et al. 1998).

3.3 Reverse lid-suture

Models explaining cortical orientation maps to emerge from correlation-based development of feedforward projections have been challenged by the outcome of reverse lid-suturing experiments (Gödecke and Bonhoeffer 1996; Sengpiel et al. 1998). In these experiments, kittens were raised so that both eyes never received visual input at the same time. This was achieved using the following protocol. Immediately after birth, one eyelid was sutured and the animal received monocular input through the other eye. After a period of a few weeks, the cortical orientation map in area 18 was recorded via optical imaging through the open eye. Then the open eye was closed and the initially closed eye was opened. After one or two weeks the second eye's orientation map in the same cortical area was measured. The two maps turned out to be nearly identical.

Assuming the activity correlations in the LGN to be determined chiefly by input from the retinae, the models predict the left-eye map and the right-eye map to develop independently of each other. Their global layouts can then be expected to be different, in striking contrast to the experimental finding.

Two different theoretical approaches have been used to explain the experimental result. The first is based on a geometric argument (Wolf et al. 1996), observing that the cat's visual area 18 is shaped into a narrow band on the cortical surface. The formation of an orientation map in this area is therefore subject to strong confinement, i.e. the layout of a developing map is predetermined by boundary conditions. Numerical simulations have confirmed that different orientation maps emerging under this condition are indeed very similar.

The second explanation relies on activity correlations in the LGN. Erwin and Miller (1998) have shown that with an appropriate amount of inter-eye correlations in the activity of geniculate relay cells, a Hebbian development of geniculocortical afferents can nicely reproduce ocularly-matched cortical orientation maps. They assume that these correlations are present in LGN activity even without visual input. Recently it has been shown that strong inter-eye correlations can in fact be found in the ferret LGN before eye opening (Weliky and Katz 1999).

It is also well-known, however, that monocular deprivation over a period of a few days during the critical period causes most cortical neurons to loose their responsiveness to stimulation of the deprived eye (Blakemore and van Sluyters 1974). As a consequence, optical imaging experiments find the orientation map of the deprived eye to be largely eliminated (Kim and Bonhoeffer 1994; Gödecke and Bonhoeffer 1996). This may indicate that LGN activity is strongly affected by monocular occlusion. According to the model of Erwin and Miller, ocularly matched orientation selectivity can

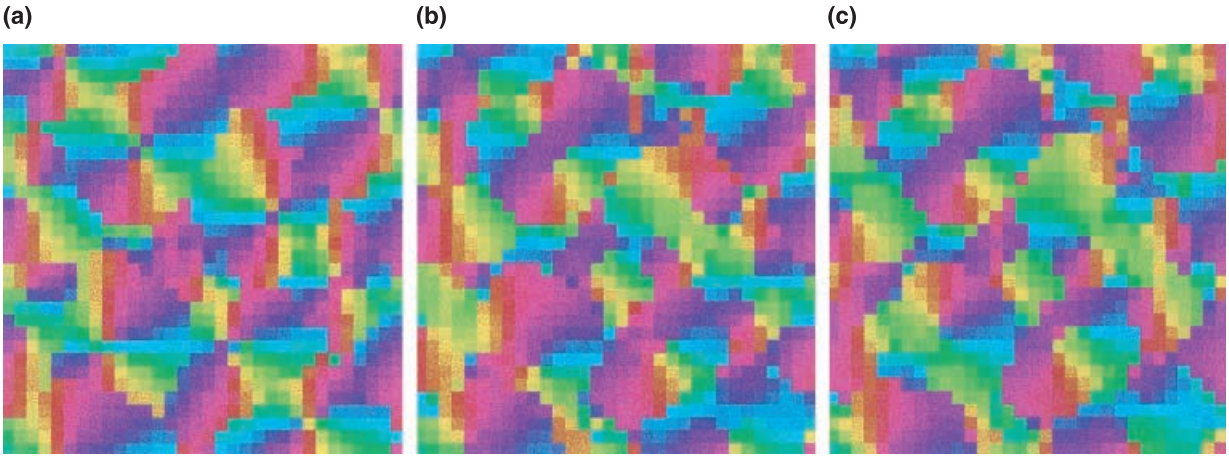

Fig. 10. The reverse lid-suturing protocol is mimicked by a sequence of numerical simulations. **a** Before the onset of geniculocortical development an intracortical orientation map is assumed to emerge from a Hebbian development of lateral connectivity in layer 4 as explained in Sect. 3.1. **b** The geniculocortical afferents of the initially-open eye are learned and produce a feedforward orientation map. **c** After the first eye has been closed, the second eye's afferents develop independently from scratch. This is simulated by re-running the feedforward learning process, but initialized with a different seed value of the random number generator. Comparing **b** and **c** reveals them to be very similar. This is in accordance with the results of reverse lid-suture experiments, in which both eyes' orientation maps have been found to be virtually identical (Gödecke and Bonhoeffer 1996; Sengpiel et al. 1998)

be maintained in a reverse-suturing experiment if one of the two following conditions is fulfilled: either the remainder of the deprived eye's map is strong enough so as to act as a seed for the restoration of the original map, or there is a sufficient amount of geniculate inter-eye correlations during the period of reverse occlusion so that the deprived map can be reinstated as a copy of the non-deprived map. It is still an open question as to whether one of these conditions does indeed hold true.

In consideration of our results presented in Sects. 3.1 and 3.2, we propose a third mechanism that may reconcile models of correlation-based geniculocortical development with experimental data. As we have shown, a Hebbian learning mechanism driven by spontaneous cortical activity may lead to the formation of an intracortical orientation map. This map is set up by lateral projections of cortical layer 4 neurons and can emerge very early in visual development – even before thalamic afferents reach cortical layer 4. The intracortical connectivity can then guide the refinement of thalamocortical inputs, so that the developing feedforward orientation map is in agreement with the intracortical map.

Let us now assume that the critical period for the development of short-range interactions in cat layer 4 ends after about three weeks postnatal. Within the framework of our model this would mean that at this time the layout of the intracortical orientation map is fixed, thereby determining the structure of both eyes' feedforward maps. The outcome of the reverse-suturing experiments can then be explained as follows.

In the course of – or possibly before – the first period of monocular deprivation, cortical layer 4 cells finish their refinement of short-range lateral connections. During the same period of time, a feedforward orientation map for the open eye emerges. Eventually the feedforward and the intracortical map are in accord with each other. Together they form the orientation map that can be recorded by means of optical imaging. After the open eye has been closed and the closed eye has been opened, cortical neurons reorganize their geniculate input synapses so that an orientation map for the newly opened eye is formed. This process is again guided by the intracortical connectivity, which does not change any more. As a consequence, the second feedforward map develops in accord with the same intracortical map as did the first one. Optical imaging at the end of the experiment therefore yields a second orientation map that is very similar to the previous one.

This mechanism can be demonstrated in the following sequence of numerical simulations. First, the Hebbian development of short-range lateral connections in cortical layer 4 is simulated according to the explanations of Sect. 3.1. This process is driven by spontaneous cortical activity and for simplicity we assume that it is finished before the onset of thalamocortical input. The emerging intracortical map is displayed in Fig. 10a.

In the presence of this intracortical map, two independent network simulations as described Sect. 3.2 are then performed to mimick the development of the two eyes' geniculocortical afferents during the reverse-suturing protocol. Starting each simulation with different seed values for the random number generator ensures that their LGN activities are uncorrelated. Despite the lack of inter-eye correlations in thalamic activity, the resulting maps are strikingly similar, as can be seen in Fig. 10b and Fig. 10c. This similarity arises because both maps develop in such a way that they are in agreement with the intracortical connectivity, which is the same during both runs.

Taken together, our results show that a patterned intracortical connectivity arising early in visual development can guide the development of feedforward

projections so that the emerging cortical orientation maps are matched in the two eyes. In our simulations, there were no inter-eye correlations in thalamic activity. This provides evidence that in the present scenario inter-eye correlations are not necessary for ocularly-matched orientation maps to develop.

4 Summary and discussion

In this paper we have introduced a neuronal model of combined lateral and geniculocortical plasticity in layer 4 of the primary visual cortex. The network consists of stochastically-spiking neurons to model geniculate relay cells as well as excitatory cortical cells interacting with inhibitory interneurons. The development of both lateral and feedforward connectivity is governed by activity-driven Hebbian learning dynamics. Plasticity of inhibitory synapses on short time-scales has been incorporated so as to stabilize cortical activity and prevent epileptiform discharges (Douglas et al. 1995; Varela et al. 1999).

We have found that in this model spontaneous cortical activity in the absence of geniculate input can drive the plasticity of lateral connections to form an intracortical orientation map. The layout of such an intracortical map resembles that of typical orientation maps obtained from optical imaging experiments in primary visual cortex. It exhibits linear zones, where orientation changes smoothly across the cortical surface, as well as so-called pinwheel centers: point-like singularities at which orientation changes discontinuously by 90 degrees (Bonhoeffer and Grinvald 1991; Blasdel 1992b).

Furthermore, a Hebbian development of geniculocortical afferents in the presence of intracortical interaction and correlated activity in the LGN leads to the emergence of orientation-selective receptive fields of cortical cells. As in previous correlation-based models of pattern formation (von der Malsburg 1973; Linsker 1986a,b; Miller 1994; Wimbauer et al. 1997a,b; Choe and Miikkulainen 1998; Erwin and Miller 1998), an isotropic pattern of intracortical connectivity is sufficient to obtain nicely ordered feedforward orientation maps that are very similar to measured ones.

We have also investigated the effect that a non-isotropic intracortical interaction in layer 4 can have on feedforward plasticity. It turned out that a previously formed intracortical orientation map can guide the development of geniculocortical afferents. As a consequence, the emerging feedforward map will be in accordance with the existing intracortical map. Comparing the lateral arborization radius of layer 4 cells in the model ($\leqslant 5.5$ cells), with the typical distance of pinwheel centers in the final orientation maps (see e.g. Fig. 10), shows that lateral interactions are normally confined to approximately one hypercolumn. The intracortical connectivity under consideration is thus short-ranged and must not be confused with the patchy patterns of horizontal projections that have been found anatomically to exist in layers 2/3 and 5 (Callaway and Katz 1990; Katz and Callaway 1992).

Since in our setup the same intracortical connectivity guides the development of afferents from both the left and the right eye, the orientation maps will be matched in the two eyes, which is in agreement with experimental data (Wiesel and Hubel 1974; Gödecke and Bonhoeffer 1996; Gödecke et al. 1997; Crair et al. 1998). It is important to note that we do not presume the response properties of cortical simple cells to be predominantly shaped by their lateral connections. Rather, we have demonstrated that the emerging pattern of feedforward connectivity is strongly influenced by an existing pattern of intracortical projections during the critical period of geniculocortical plasticity. As a result, both eye's orientation maps will be very similar, no matter whether orientation selectivity is established mainly by lateral or by feedforward connections, or by both. As we have shown, this may provide a new explanation for the outcome of reverse lid-suturing experiments (Gödecke and Bonhoeffer 1996; Sengpiel et al. 1998). In contrast to earlier propositions (Wolf et al. 1996; Erwin and Miller 1998) it is neither dependent on the geometry of the respective cortical area nor on inter-eye correlations in thalamic activity.

Further support for our model comes from recent observations of Sengpiel et al. (1999). They raised kittens in an environment where they could see contours of only one orientation. The orientation maps that were obtained from these animals via optical imaging exhibited only a moderate shift towards this orientation. This is in full agreement with a scenario in which the development of geniculocortical afferents is guided by an existing pattern of intracortical connectivity and visual experience has an only minor influence.

Current anatomical data (Shatz and Luskin 1986; Gosh and Shatz 1992) show that, in the cat, geniculate afferents reach layer 4 of the primary visual cortex about one week after the cells in this layer have finished their migration. This raises the possibility that these cells start an activity-driven development of lateral interactions at least one week before a Hebbian modification of feedforward afferents can begin. Although in the present paper we have focused on the case of intracortical learning occurring strictly before geniculocortical refinement, the above considerations remain valid in a scenario in which both types of connections develop jointly for a certain period of time. The crucial requirement is that the plasticity of short-ranged lateral synapses in layer 4 ceases relatively early so that (i) the emerging intracortical map is independent of visual experience and (ii) the feedforward afferents can adapt to this map.

We know of only one other spiking network model dedicated to the problem of combined development of feedforward and lateral projections (Choe and Miikkulainen 1998). In contrast to the aim of the present work, however, these authors did not analyze the possibility of an intracortical map formation and its implications for the refinement of geniculocortical afferents. Rather, they concentrated on the formation of feedforward maps and the role that fast-adapting intracortical synapses can take in the segmentation of visual scenes afterwards.

Since our network is made up of spiking neurons and distinguishes strictly between excitatory cells and inhibitory interneurons, it is closer to biology than many previous models of the visual cortex. We have verified that this relatively detailed approach can reproduce earlier results on the formation of orientation maps. This was not obvious a priori because stochastically-spiking networks produce noise which may prevent ordered receptive fields from developing within biologically plausible time scales.

Quite to the contrary and most importantly, we have demonstrated that the new synaptic order, i.e. the intracortical orientation map, is due to inherent cortical noise. An external source of noise would be necessary to obtain similar results in a network consisting of the usual graded-response neurons. The similarity of such intracortical maps to optically recorded maps of preferred orientation, and the finding that they can guide the refinement of feedforward afferents, emphasizes the role of horizontal connections in shaping neuronal response properties. Not only are lateral interactions likely to modulate a cortical cell's tuning curve 'on the run', they can even predetermine its input connectivity during development.

Acknowledgement. A. P. B. gratefully acknowledges support by the Graduiertenkolleg 'Sensorische Interaktion in biologischen und technischen Systemen' in Munich.

Appendix A: Simulation parameter values

In order to allow the reader to reproduce the results presented in this paper, we list the relevant simulation parameters in this appendix. A description of the simulation algorithm is given in Sect. 2.2.

A.1 Intracortical plasticity

We have assumed that the refinement of short-ranged connections within cortical layer 4 occurs before the onset of geniculocortical input. For the corresponding simulations the geniculate layer has thus been removed from our network (Fig. 1). The remaining cortical part consists of excitatory neurons and inhibitory interneurons arranged on two equally sized square grids. For the firing probability (Eq. 1), $\theta = 3$ and $T = 0.5$ for both excitatory cells and inhibitory neurons.

Within a circular arborization region of 11 neurons in diameter, the excitatory neurons connect to one another as well as to the inhibitory neurons, and the latter project back to the excitatory cells. Thus there is no connection between two cells if the distance of their grid positions is larger than 11/2.

Within this radius the connections from excitatory to inhibitory neurons are kept at fixed values

$$J_{ij} = 0.3 \exp\left[-\mathrm{d}(i,j)^2/\left(2 \cdot 3^2\right)\right] ,$$

with $\mathrm{d}(i,j)$ denoting the distance between the grid positions of inhibitory neuron i and excitatory neuron j.

In contrast, the synapses between excitatory cells and those from inhibitory to excitatory neurons are plastic. They develop according to the learning rules described in Sect. 2.3. We use Gaussian-shaped arbor functions

$$A^{\mathrm{e}}_{ij} = 0.025 \exp\left[-\mathrm{d}(i,j)^2/\left(2 \cdot 3^2\right)\right] ,$$
$$A^{\mathrm{i}}_{ij} = 0.05 \exp\left[-\mathrm{d}(i,j)^2/\left(2 \cdot 3^2\right)\right] ,$$

where $\mathrm{d}(i,j)$ denotes again the distance between the grid positions of the respective neurons. An upper limit $J^{\max} = 0.8$ is applied for the weight of excitatory synapses. Furthermore, we let $\sigma_i = 1$ in Eq. 6. The values of the remaining parameters σ^{e}, ξ^{e} and the grid size are varied from run to run. They are summarized in Table A1.

Table A1. Each row specifies the quantities σ^{e}, ξ^{e}, the total number of simulated time steps, and the grid size for one network run simulating Hebbian development of intracortical connections. The values are listed together with the number of the figure that presents the corresponding results. All the other simulation parameters are held constant as given in Sect. A.1. Parameter sets #3 and #4 are equal except for the seed value of the random number generator

#	Figure	Grid size	Time steps	σ^{e}	ξ^{e}
1	6a	16×16	$2.5 \cdot 10^6$	−0.57	$8.0 \cdot 10^{-4}$
2	6b,c	16×16	$2.5 \cdot 10^6$	−0.57	$9.5 \cdot 10^{-4}$
3	7, 9a	32×32	$2.5 \cdot 10^6$	−0.57	$9.5 \cdot 10^{-4}$
4	10a	32×32	$2.5 \cdot 10^6$	−0.57	$9.5 \cdot 10^{-4}$

A.2 Geniculocortical plasticity

For our simulations of geniculocortical development we use the full network presented in Fig. 1. The grid size is 32×32. We fix the excitatory intracortical connectivity, while we let excitatory feedforward and inhibitory intracortical synapses develop according to (4) and (6), respectively.

The postsynaptic potential $\varepsilon(t)$ and the refractory potential $\eta(t)$ are set as given in (2) and (3). For the firing probability we use again (1) but with $\theta = 13$ and $T = 0.25$ for excitatory cells, and $\theta = 3$ and $T = 0.25$ for inhibitory neurons.

At the very early developmental stage that we are concerned with, real cortical cells are still in a process of maturation, i.e. their response properties are very likely to change with time. Thus, there is no need to assume that the response properties of our model neurons, i.e. θ and T, are constant.

The spatiotemporal activity correlations in the geniculate layer that are required to drive thalamocortical pattern formation are generated as follows. After every ten simulated time steps, the membrane potentials h_i of all the neurons i on the thalamic layer are drawn as a new realization of a Gaussian random field and are then kept fixed over the subsequent ten iterations. Each geniculate cell produces a random spike train according to its membrane potential and the firing probability (1) with $\theta = 7$, $T = 1$.

In order to describe the Gaussian random field of membrane potentials, the expectation values $\langle h_i \rangle$ as well as the correlation matrix $\langle h_i h_j \rangle$ must be given. Throughout this paper, we have set $\langle h_i \rangle = 0$ and

$$\langle h_i h_j \rangle = 16.3 \exp\left[-\mathrm{d}(i,j)^2/\left(2 \cdot 1^2\right)\right] - 1.82 \exp\left[-\mathrm{d}(i,j)^2/\left(2 \cdot 3^2\right)\right] ,$$

which is a Mexican-hat-like function of the distance $\mathrm{d}(i,j)$ between the respective geniculate neurons i and j.

The parameters governing the dynamics of inhibitory weights are the same as specified in Sect. A.1. For the development of feedforward synapses, we use an arbor function

$$A^{\mathrm{e}}_{ij} = 0.0125 \exp\left[-\mathrm{d}(i,j)^2/\left(2 \cdot 3^2\right)\right] ,$$

and apply an upper weight limit $J^{\max} = 1$.

Table A2. For each simulation of geniculocortical development, the network parameters σ^e and ξ^e, the total number of simulated time steps, and the corresponding figures are listed. In addition, the lateral excitatory connectivity is specified in the following way. If the pattern of lateral weights is isotropic, then the amplitude J_0^{ic}, corresponding to (A1), is given. If the connectivity pattern is the result of a previous simulation of intracortical development, then we indicate that simulation by specifying the corresponding row of Table 1. The last two parameter sets are identical except for the seed value of the random number generator

Figure	Time steps	σ^e	ξ^e	J_0^{ic}	# in Table 1
8b,c	$5 \cdot 10^6$	0.85	$8 \cdot 10^{-4}$	0.7	–
9b	$5 \cdot 10^6$	0.4	$8 \cdot 10^{-4}$	–	3
10b	$5 \cdot 10^6$	0.4	$8 \cdot 10^{-4}$	–	4
10c	$5 \cdot 10^6$	0.4	$8 \cdot 10^{-4}$	–	4

Table A2 lists the values of those parameters that are varied in the different simulations. During each simulation the excitatory lateral weights are kept constant. Their values are either taken from a previous simulation of intracortical development or determined by the Gaussian

$$J_{ij} = J_0^{ic} \exp\left[-d(i,j)^2/(2 \cdot 3^2)\right] , \qquad (A1)$$

where $d(i,j)$ is the distance between the two cortical cells i and j. In the former case, Table A2 references the corresponding intracortical simulation by its respective number in Table A1. In the latter case, the value of J_0^{ic} is given.

References

Bartsch AP, van Hemmen JL (1999) Development of orientation maps from Hebbian learning of intracortical connections. In: Elsner N, Eysel U (eds) Göttingen Neurobiology Report, Volume II. Georg Thieme Verlag, Stuggart, p 502

Bartsch AP, van Hemmen JL (2000) Analysis of pattern formation in a network of spiking neurons with non-isotropic lateral connections: development of orientation maps. In preparation

Blakemore C, van Sluyters RC (1974) Reversal of the physiological effects of monocular deprivation in kittens: further evidence for a sensitive period. J Physiol (Lond) 237: 195–216

Blasdel GG (1992a) Differential imaging of ocular dominance and orientation selectivity in monkey striate cortex. J Neurosci 12: 3115–3138

Blasdel GG (1992b) Orientation selectivity, preference, and continuity in monkey striate cortex. J Neurosci 12: 3139–3161

Blasdel GG, Salama G (1986) Voltage-sensitive dyes reveals a modular organization in the monkey striate cortex. Nature 321: 579–585

Bonhoeffer T, Gödecke I (1996) Organization of the visual cortex – reply. Nature 382: 306–307

Bonhoeffer T, Grinvald A (1991) Iso-orientation domains in cat visual cortex are arranged in pinwheel-like patterns. Nature 353: 429–431

Bonhoeffer T, Grinvald A (1993) The layout of iso-orientation domains in area 18 of cat visual cortex: optical imaging reveals a pinwheel-like organization. J Neurosci 13: 4157–4180

Bosking WH, Zhang Y, Schofield B, Fitzpatrick D (1997) Orientation selectivity and the arrangement of horizontal connections in tree shrew striate cortex. J Neurosci 17: 2112–2127

Braitenberg V, Schüz A (1991) Anatomy of the cortex. Springer, Berlin Heidelberg New York

Brown TH, Chattarji S (1994) Hebbian synaptic plasticity: evolution of the contemporary concept. In: Domany E, van Hemmen JL, Schulten K (eds) Models of Neural Networks II. Springer, Berlin Heidelberg New York, pp 287–314

Callaway EM, Katz LC (1990) Emergence and refinement of clustered horizontal connections in cat striate cortex. J Neurosci 10: 1134–1153

Chapman B, Stryker MP (1993) Development of orientation selectivity in ferret visual cortex and effects of deprivation. J Neurosci 13: 5251–5262

Chapman B, Stryker MP, Bonhoeffer T (1996) Development of orientation preference maps in ferret primary visual cortex. J Neurosci 16: 6443–6453

Choe Y, Miikkulainen R (1998) Self-organization and segmentation in a laterally connected orientation map of spiking neurons. Neurocomputing 21: 51–60

Chung S, Ferster D (1998) Strength and orientation tuning of the thalamic input to simple cells revealed by electrically evoked cortical suppression. Neuron 20: 1177–1189

Crair MC, Gillespie DC, Stryker MP (1998) The role of visual experience in the development of columns in cat visual cortex. Science 279: 566–570

Crook JM, Eysel UT (1992) GABA-induced inactivation of functionally characterized sites in cat visual cortex (area 18): effects on orientation tuning. J Neurosci 12: 1816–1825

Douglas RJ, Koch C, Mahowald M, Martin KAC, Suarez HH (1995) Recurrent excitation in neocortical circuits. Science 269: 981–985

Engert F, Bonhoeffer T (1997) Synapse specificity of long-term potentiation breaks down at short distances. Nature 388: 279–284

Engert F, Bonhoeffer T (1999) Dendritic spine changes associated with hippocampal long-term synaptic plasticity. Nature 399: 66–70

Erwin E, Miller KD (1998) Correlation-based development of ocularly-matched orientation and ocular dominance maps: determination of required input activities. J Neurosci 18: 9870–9895

Ferster D (1987) Origin of orientation-selective EPSPs in simple cells of cat visual cortex. J Neurosci 7: 1780–1791

Ferster D (1988) Spatially opponent excitation and inhibition in simple cells of the cat visual cortex. J Neurosci 8: 1172–1180

Ferster D, Chung S, Wheat H (1996) Orientation selectivity of thalamic input to simple cells of cat visual cortex. Nature 380: 249–252

Ferster D, Miller KD (2000) Neural mechanisms of orientation selectivity in the visual cortex. Annu Rev Neurosci 23: 441–471

Fregnac Y, Burke JP, Smith D, Friedlander MJ (1994) Temporal covariance of pre- and postsynaptic activity regulates functional connectivity in the visual cortex. J Neurophysiol 71: 1403–1421

Gerstner W, van Hemmen JL (1992) Associative memory in a network of 'spiking' neurons. Network 3: 139–164

Gerstner W, van Hemmen JL (1994) Coding and information processing in neural networks. In: Domany E, van Hemmen JL, Schulten K (eds) Models of Neural Networks II. Springer, Berlin Heidelberg New York, pp 1–93

Gödecke I, Bonhoeffer T (1996) Development of identical orientation maps for two eyes without common visual experience. Nature 379: 251–254

Gödecke I, Kim DS, Bonhoeffer T, Singer W (1997) Development of orientation preference maps in area 18 of kitten visual cortex. Eur J Neurosci 9: 1754–1762

Gosh A, Shatz CJ (1992) Pathfinding and target selection by developing geniculocortical axons. J Neurosci 12: 39–55

Hebb DO (1949) The organization of behavior. Wiley, New York

Hubel DH, Wiesel TN (1962) Receptive fields, binocular interaction and functional architecture in the cat's visual cortex. J Physiol (Lond) 160: 106–154

Hubel DH, Wiesel TN, Stryker MP (1977) Orientation columns in macaque monkey visual cortex demonstrated by the 2-deoxyglucose autoradiographic technique. Nature 269: 328–330

Humphrey AL, Norton TT (1980) Topographic organization of the orientation column system in the striate cortex of the tree

shrew (tupaia glis). I. Microelectrode recording. J Comp Neurol 192: 531–547
Humphrey AL, Skeen LC, Norton TT (1980) Topographic organization of the orientation column system in the striate cortex of the tree shrew (tupaia glis). II. deoxyglucose mapping. J Comp Neurol 192: 549–566
Issa NP, Trachtenberg JT, Chapman B, Zahs KR, Stryker MP (1999) The critical period for ocular dominance plasticity in the ferret's visual cortex. J Neurosci 19: 6965–6978
Kammen DM, Yuille AL (1988) Spontaneous symmetry-breaking energy functions and the emergence of orientation selective cortical cells. Biol Cybern 59: 23–31
Katz LC, Callaway EM (1992) Development of local circuits in mammalian visual cortex. Annu Rev Neurosci 15: 31–56
Kim DS, Bonhoeffer T (1994) Reverse occlusion leads to a precise restoration of orientation preference maps in visual cortex. Nature 370: 370–372
Law MI, Zahs KR, Stryker MP (1988) Organization of primary visual cortex (area 17) in the ferret. J Comp Neurol 278: 157–180
LeVay S, Hubel DH, Wiesel TN (1975) The pattern of ocular dominance columns in macaque visual cortex revealed by a reduced silver stain. J Comp Neurol 159: 559–576
Linsker R (1986a) From basic network principles to neural architecture: emergence of orientation columns. Proc Natl Acad Sci USA 83: 8779–8783
Linsker R (1986b) From basic network principles to neural architecture: emergence of orientation selective cells. Proc Natl Acad Sci USA 83: 8390–8394
von der Malsburg C (1973) Self-organization of orientation selective cells in the striate cortex. Kybernetika 14: 85–100
Markram H, Lübke J, Frotscher M, Sakmann B (1997) Regulation of synaptic efficacy by coincidence of postsynaptic AP and EPSP. Science 275: 213–215
Miller KD (1994) A model for the development of simple cell receptive fields and the ordered arrangement of orientation columns through activity-dependent competition between ON- and OFF-center inputs. J Neurosci 14: 409–441
Miller KD, Erwin E, Kayser A (1999) Is the development of orientation selectivity instructed by activity? J Neurobiol 41: 44–57
Nelson S, Toth L, Sheth B, Sur M (1994) Orientation selectivity of cortical neurons during intracellular blockade of inhibition. Science 265: 774–777
Reid RC, Alonso JM (1995) Specificity of monosynaptic connections from thalamus to visual cortex. Nature 378: 281–284
Sengpiel F, Gödecke I, Stawinski P, Hübener M, Lowel S, Bonhoeffer T (1998) Intrinsic and environmental factors in the development of functional maps in cat visual cortex. Neuropharmacology 37: 607–621
Sengpiel F, Stawinsky P, Bonhoeffer T (1999) Influence of experience on orientation maps in cat visual cortex. Nature Neurosci 2: 727–732
Shatz CJ, Luskin MB (1986) The relationship between the geniculocortical afferents and their cortical target cells during development of the cat's primary visual cortex. J Neurosci 6: 3655–3668
Sillito AM (1979) Inhibitory mechanisms influencing complex cell orientation selectivity and their modification at high resting discharge levels. J Physiol (Lond) 289: 33–53
Sillito AM, Kern JA, Milson JA, Berardi N (1980) A re-evaluation of the mechanisms underlying simple cell orientation selectivity. Brain Res 194: 517–520
Stetter M, Lang EW, Müller A (1993) Emergence of orientation selective simple cells simulated in deterministic and stochastic neural networks. Biol Cybern 68: 465–476
Turrigiano GG, Leslie KR, Desai NS, Rutherford LC, Nelson SB (1998) Activity-dependent scaling of quantal amplitude in neocortical neurons. Nature 391: 892–896
Tusa RJ, Palmer LA, Rosenquist AC (1978) The retinotopic organization of area 17 (striate cortex) in the cat. J Comp Neurol 177: 213–235
Varela JA, Song S, Turrigiano GG, Nelson SB (1999) Differential depression at excitatory and inhibitory synapses in visual cortex. J Neurosci 19: 4293–4304
Vidyasagar TR, Pei X, Volgushev M (1996) Multiple mechanisms underlying the orientation selectivity of visual cortical neurones. Trends Neurosci 19: 272–277
Weliky M, Katz LC (1997) Disruption of orientation tuning in visual cortex by artificially correlated neuronal activity. Nature 386: 680–685
Weliky M, Katz LC (1999) Correlational structure of spontaneous neuronal activity in the developing lateral geniculate nucleus in vivo. Science 285: 599–604
Wiesel TN, Hubel DH (1963) Single-cell responses in striate cortex of kittens deprived of vision in one eye. J Neurophysiol 26: 1003–1017
Wiesel TN, Hubel DH (1974) Ordered arrangement of orientation columns in monkeys lacking visual experience. J Comp Neurol 158: 307–318
Wimbauer S, Wenisch OG, van Hemmen JL, Miller KD (1997a) Development of spatiotemporal receptive fields of simple cells: II. simulation and analysis. Biol Cybern 77: 463–477
Wimbauer S, Wenisch OG, Miller KD, van Hemmen JL (1997b) Development of spatiotemporal receptive fields of simple cells: I. model formulation. Biol Cybern 77: 453–461
Wolf F, Bauer HU, Pawelzik K, Geisel T (1996) Organization of the visual cortex. Nature 382: 306–307
Zhang LI, Tao HW, Holt CE, Harris WA, Poo MM (1998) A critical window for cooperation and competition among developing retinotectal synapses. Nature 395: 37–44